Available online at www.sciencedirect.com
SCIENCE DIRECT
Journal of Catalysis 239 (2006) 187–199
JOURNAL OF CATALYSIS
www.elsevier.com/locate/jcat

Dissociative adsorption of CH_4 on NiAu/YSZ: The nature of adsorbed carbonaceous species and the inhibition of graphitic C formation

Nikolaos C. Triantafyllopoulos, Stylianos G. Neophytides *

Institute of Chemical Engineering & High-Temperature Processes, GR-26500 Patras, Greece

Received 1 November 2005; revised 13 January 2006; accepted 13 January 2006

Available online 28 February 2006

Abstract

Methane dissociative adsorption and partial oxidation reaction were studied by means of adsorption equilibrium and transient experiments on Au-modified Ni/YSZ powders. It was found that the addition of 1% atomic ratio of Au with respect to Ni on Ni/YSZ cermet catalyst (total metal loading 50 wt%) significantly affects both the kinetics of CH_4 dissociative adsorption and the binding strength of the adsorbed CH_x species on the Ni surface. The formation of graphitic carbon is significantly inhibited, whereas the hydrogenation of CH_x species into CH_4, studied by means of temperature-programmed reaction spectroscopy (TPRS), occurs at temperatures 100 K higher than on the unmodified Ni/YSZ surface. This implies higher stability and elongation of the CH_x species lifetime on the NiAu/YSZ surface before their decomposition into surface carbidic species. The oxidation reactions involve both the oxidation of CH_x species into CH_xO and its subsequent decomposition at elevated temperatures (700 K) into CO and H_2, whereas carbidic species are selectively oxidized into CO_2 at temperatures as low as 500 K. In this respect, the higher CH_x surface concentration on the Au-modified Ni/YSZ species will result in higher selectivity toward the production of synthesis gas, with greatly suppressed graphitic carbon formation.

Keywords: CH_4 dissociation; Gold; NiAu/YSZ; SOFC; Partial oxidation of methane

1. Introduction

Electrochemical methane oxidation in solid oxide fuel cells (SOFCs) has received considerable attention for both its complete oxidation and the cogeneration of synthesis gas and electric power [1–9]. In general, the electrochemical oxidation of methane can be described as

$$CH_4, CO_2, CO, H_2, M|(ZrO_2\ 8\ mol\%\ Y_2O_3)|M', air. \quad (1)$$

Oxygen ions, O^{2-}, are formed on the air cathode electrode (M′) and are readily transferred to the anode electrode catalyst (M) through the YSZ electrolyte. On the anode, they can be either discharged, forming oxygen, or oxidize methane.

Electrochemical oxidation of methane to synthesis gas has several advantages over catalytic oxidation of methane [2,3,5]. It enables the simultaneous production of synthesis gas and electricity, thus combining the concepts of a chemical reactor and power generator. Because CH_4 and O_2 (air) are separated by the YSZ electrolyte, the danger of the formation of an explosive reaction mixture or the development of hot spots in the reactor by the highly exothermic complete oxidation is diminished. When air is used as an oxidant, nitrogen does not accumulate in the final product, because oxygen is separated from nitrogen at the cathode, that is, at the stage when it is fed to the reaction zone. In this respect, the studies in this field are quite interesting and attractive both to elucidate the feasibility of the electrocatalytic conversion of methane to synthesis gas and to develop the natural gas-fueled SOFC capable of cogenerating electricity and synthesis gas.

In principle, an SOFC can operate on any combustible fuel that can react with oxide ions pumped through the electrolyte onto the anode. Toward this direction, the synthesis and development of electrocatalytically active anodes for the CH_4 oxidation are important to the design and development of SOFCs capable of direct electrocatalytic oxidation of methane and other hydrocarbons.

* Corresponding author. Fax: + 30 2610 965223.
E-mail address: neoph@iceht.forth.gr (S.G. Neophytides).

0021-9517/$ – see front matter
doi:10.1016/j.jcat.2006.01.021

In this context, the Ni/YSZ cermet anode is the most popular electrocatalyst for both H_2 and CH_4 oxidation [5,7,9–11]. In practice, the high operating temperatures (>870 K) in the presence of hydrocarbons can lead to carbon formation on the Ni/YSZ anode, resulting in rapid degradation of the electrode. Carbon deposition occurs through the catalytic dissociative adsorption of CH_4 on the anode electrode surface [12–14],

$$CH_4 \rightarrow C_{gr} + 2H_2. \quad (2)$$

One approach to avoid carbon formation using the conventional Ni/YSZ cermet anode is to operate the fuel cell under modified operating conditions, that is, intermediate temperatures with continuous current flow in the presence of steam [1,7,10]. However, the addition of a high steam:CH_4 ratio (2:1) reaction mixture results in partial oxidation of the Ni/YSZ anode and, according to Nerst's equation, reduction of its open circuit potential (OCP). This results in poorer performance of the Ni/YSZ anode and a negative effect on its oxidative stability. Thus, a long-sought goal for the successful implementation of SOFC technology is the synthesis and development of CH_4-exposed carbon-tolerant anodes.

Toward this direction, Ni-based anodes exhibit analogous behavior to the steam-reforming supported nickel catalysts. Several studies have shown that the addition of alkali [15–17] or other metals [18–22] reduces carbon formation under methane-reforming reactions. Borowiecki et al. [18,19] have shown that adding 1 wt% Mo to the supported Ni catalysts significantly reduced carbon deposition. Another previous study found that the presence of small quantities of Mo (1 wt%) on Ni/YSZ suppressed the formation of adsorbed graphitic layers during the dissociative adsorption of CH_4 [21]. However, as predicted theoretically and observed experimentally, the most promising behavior toward increased carbon tolerance of the Ni surface was obtained by adding small amounts of Au (<0.1 Ni surface coverage) with respect to Ni loading on Ni/Al_2O_3 catalysts [22].

In the light of the aforementioned theoretical and experimental considerations, the aim of this paper is to elucidate the role of adding Au on Ni/YSZ cermet in terms of the formation and nature of the various carbon adspecies on the NiAu/YSZ surface and the surface kinetic mechanism for the partial oxidation of CH_4 by means of thermodynamic equilibrium measurements and temperature-programmed desorption and reaction spectroscopy.

2. Experimental

2.1. Ni/YSZ and NiAu/YSZ preparation and characterization

YSZ was prepared by the sol–gel method starting from the hydrolysis of zirconium tetra-*n*-butoxide and the subsequent addition of yttrium nitrate hexahydrate. Sol preparation was done as described previously [21]. $Ni(NO_3)_2$ and $HAuCl_4$ were added in the final sol of ZrO_2 and Y_2O_3 to obtain a final product with 50 wt% Ni and Au atomic ratios of 0.2 and 1 at% with respect to Ni. After drying, the final powders were calcined under O_2(20%)/He flow (100 cc STP/min) at 1173 K, at a rate of 20 K/min, for 1 h. Before use, the catalysts were reduced under H_2(5%)/Ar flowing atmosphere at a total flow rate of 150 cc STP/min. The temperature was ramped at a rate of 20 K/min up to 1123 K and kept there for 1 h.

BET and specific surface areas were measured using a QuantaChrome Autosorb-1 BET and chemisorption system, and XPS analysis was carried out in a UHV equipped with a hemispherical analyzer (SPECS LH-10) and a twin-anode X-ray gun. For the in situ measurement of specific surface area, CO uptake was measured by injecting calibrated CO pulses through the catalyst bed by means of a 1-cc sample loop (Fig. 1). Ar served as the carrier gas (30 cc STP/min), and CO mole fraction was monitored with a quadrapole mass spectrometer (Balzers Omnistar). CO was injected several times until no signifi-

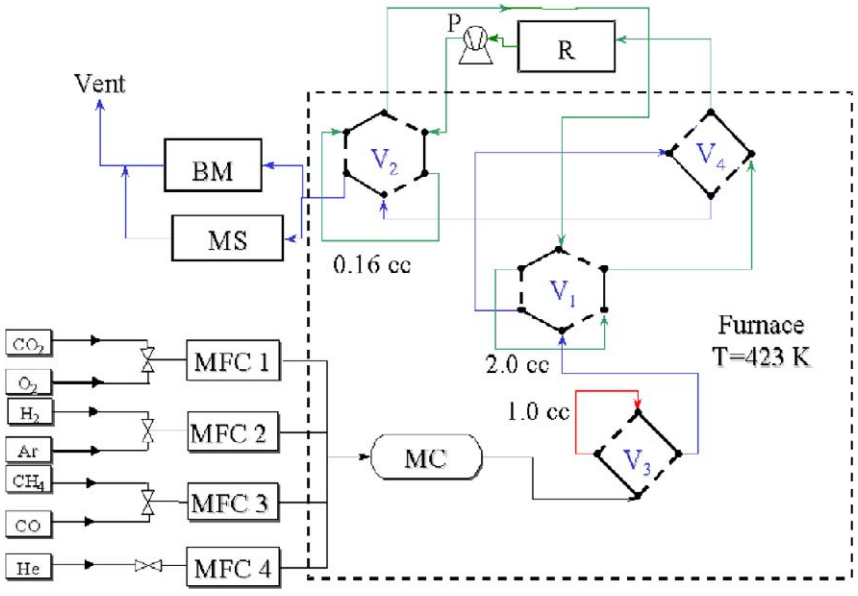

Fig. 1. Flow sheet of the experimental setup. R: reactor, P: recirculation pump, V_1–V_4: chromatographic valves, MFC: mass flow controllers, MC: mixing chamber, MS: quadrupole mass spectrometer, BM: Bubble flow meter.

cant difference could be seen in the areas of CO peaks eluted. Comparing the amount of CO detected by mass spectrometry with the amount of CO injected into the system yielded the quantity of CO adsorbed on the catalysts. Ni/Au particle size was measured by XRD (Philips PW18). The calculation was based on X-ray line broadening of the diffraction peak according to Scherrer's equation. Temperature-programmed reduction experiments were performed using a TA Instruments thermogravimetric analyzer under H_2 flow with a temperature ramp rate of 20 K/s.

2.2. Thermodynamic equilibrium experiments

The experimental procedures for equilibrium adsorption and transient experiments were as described previously [21]. Here we give only a brief description of these procedures. Fig. 1 shows a schematic diagram of the experimental setup. Thermodynamic studies were carried out in a closed reactor loop. A KNF Neuberger diaphragm pump was used to circulate gas inside the closed loop, to ensure good mixing and uniform gas-phase composition in the catalytic bed (Fig. 1). The experiments were carried out in a temperature range of 573–973 K. The catalyst loading in the quartz tube reactor was 0.8 g for Ni(Au 0.2 at%)/YSZ and 1.0 g for Ni(Au 1.0 at%)/YSZ, and the initial amount of CH_4 injected into the reactor loop varied between 3 and 60 μmol. The reactor outlet was monitored using a Balzers Omnistar quadrupole mass spectrometer.

2.3. Temperature-programmed experiments

The carbon species formed on the catalytic surface were removed by temperature-programmed surface reaction (TPSR) under H_2/Ar flow or by temperature-programmed oxidation (TPO) of the surface carbon. For the TPSR experiments, the reactor was cooled at room temperature under an Ar stream and then heated from 300 K to 1123 K in a flow of 2% H_2/Ar (152 cc STP/min) at a ramp rate of 20 K/min. For the TPO experiments, the reactor loop was purged with Ar and cooled, and at temperatures below 473 K pulses of O_2 were injected into the catalytic bed through a four-port valve (Fig. 1). The total amount of O_2 adsorbed on the catalyst surface was controlled so that the resulting O_2/(surface carbon) ratio was equal to 2. Thereafter, the reactor was linearly heated under Ar flow (30 cc STP/min) to 1123 K at a ramp rate of 20 K/min. The products of both procedures were recorded as a function of temperature by a quadrupole mass spectrometer (Balzers Omnistar).

2.4. Pulse experiments

Pulse experiments were carried out to confirm the conclusions drawn regarding the surface reactions' scheme for CH_4 partial oxidation into synthesis gas. Although transient pulse experiments are not sufficient to reach final conclusions regarding the steady-state catalytic activity, nevertheless information can be extracted concerning the reaction mechanism and the nature of the surface species responsible for the production of certain products by comparing their evolution time and their distribution at the reactor outlet. In the present case, these transient pulse experiments could be carried out either by introducing a pulse of CH_4 and O_2 through the reactor or by preadsorbing O_2 and pulsing only CH_4. The second choice can give a clearer picture due to the smaller number of processes involved, because O_2 is already adsorbed on the Ni/YSZ surface. To control the initial oxygen coverage on the Ni surface, a certain amount of oxygen was preadsorbed on the Ni/YSZ surface, and then a certain amount of CH_4 was pulsed through the Ni/YSZ catalytic bed while the reactor outlet was continuously monitored by a quadrupole mass spectrometer. A 50-mg sample of Ni/YSZ catalyst was used, and the preadsorbed O_2 coverage on the surface was formed by pulsing 2.1 and 4.4 μmol O_2. The amount of CH_4 pulsed was 2.2 μmol in both cases.

3. Results

3.1. Physicochemical properties of Ni/Au-YSZ

As mentioned in Section 2, the physicochemical characterization of the two NiAu/YSZ samples was based on BET and chemisorption measurements of surface area, whereas conclusions on the chemical and structural states were based on XPS and XRD measurements. Table 1 shows the measured surface areas and H_2 and CO uptakes of the two Ni/Au catalysts. The BET surface area is within experimental error for both samples, in accordance with the similar particle sizes of the two samples, as measured by XRD. In the case of H_2 chemisorption, the measured Ni active surface area appears to be lower in the sample with the higher gold content, which can be attributed to the screening of the Ni surface by the Au particles. This finding is corroborated by the XPS measurements showing that Au is accumulated on the surface; in the two samples, the estimated Au content is three times higher than the nominal content (Table 2).

CO uptake measurements before, during, and after the experiments (Table 1) showed that the two catalysts exhibited no alterations in surface area during or after the equilibrium

Table 1
BET surface areas and H_2 and CO uptakes of Ni/Au-YSZ catalysts

Ni/Au-YSZ	S_{BET} (m^2/g)	H_2 uptake (μmol/g)	CO uptake (μmol/g)		C from TPSR (μmol/g)	Particle size (nm)	
			Fresh catalyst	End of experiment		Ni[a]	YSZ[a]
0.2 at% Au	7.6	35.1	21.9	21.3	20.5	20.2	29.3
1.0 at% Au	7.2	25.2	5.9	5.4	5.1	20.3	29.4

[a] Determined from Ni(011) and YSZ(111) reflections according to the Scherrer equation.

Table 2
Surface composition of Ni/Au-YSZ catalysts based on XPS

Ni/Au-YSZ	Nominal composition (wt%)					Calculated composition (wt%)				
	Ni	Au	Zr	Y	O	Ni	Au	Zr	Y	O
0.2 at% Au	49.9	0.23	31.8	5.4	12.7	52.4	0.44	22.3	5.5	19.3
1.0 at% Au	49.4	1.17	31.5	5.3	12.6	40.2	3.25	23.2	2.3	30.9

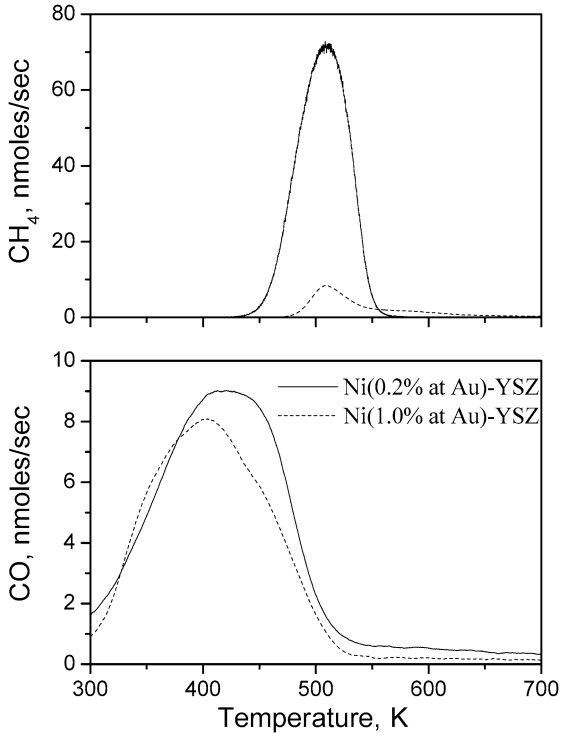

Fig. 2. Temperature-programmed surface reaction (TPSR) following CO chemisorption at r.t. on Ni(Au 0.2 at%)/YSZ and Ni(Au 1.0 at%)/YSZ under 2.5% H_2/Ar flow. Total flow rate 167 cc STP/min, ramp rate 20 K/min.

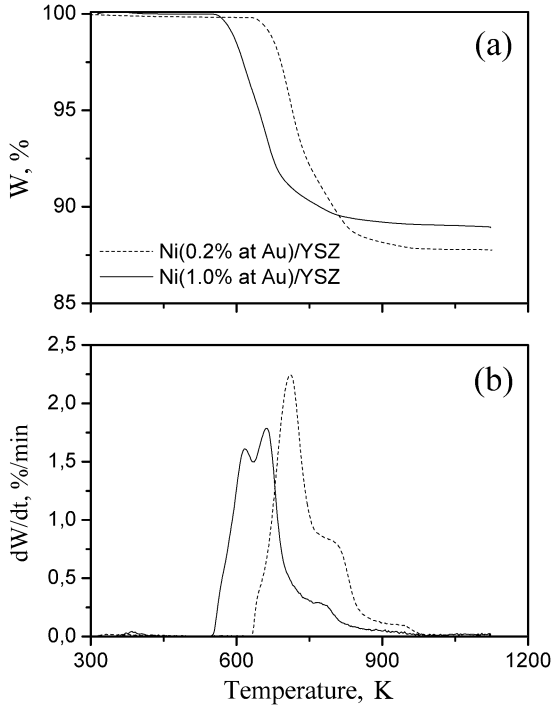

Fig. 3. Temperature-programmed reduction (TPR) by means of thermal gravimetric analysis (TGA) under 7.7% H_2/Ar, flow rate = 65 cc STP/min, ramp rate = 20 K/min.

CH_4 adsorption and transient reaction experiments. However, the measured CO uptake differed significantly from the corresponding H_2 chemisorption experiments, especially for the high-Au content sample (Table 1). To gain a deeper insight into this discrepancy, TPSR experiments were carried out under H_2/Ar flow after CO chemisorption using the conditions described in Section 2. These experiments are depicted in Fig. 2 for both samples, and the main observations can be summarized as follows:

1. Similar amounts of CO desorb from both samples and within the same temperature range (Fig. 2).
2. The evolved CH_4 originates from the hydrogenation of adsorbed CO/C species and exhibits the same peak maximum but a different peak temperature distribution between the two samples. Most significantly, the amount of CH_4 formation on Ni(Au 1.0 at%)/YSZ is an order of magnitude smaller than the corresponding amount formed on Ni(Au 0.2 at%)/YSZ.
3. Small amounts of CO_2 and water are formed mainly on Ni(Au 0.2 at%)/YSZ.
4. As shown in Table 1, the total amount of CO uptake measured during the CO pulses is equal (within experimental error) to the amount of carbon extracted by the TPSR experiment. In this respect, any possible formation of $Ni(CO)_4$ [23] is considered negligible and does not affect the measured CO uptake shown in Table 1.

These observations lead to the conclusion that Ni(Au 1.0 at%)/YSZ is far less active for CO hydrogenation/methanation reaction by affecting either CO chemisorption or CO dissociation toward the formation of carbidic species that are reactive with H_2 toward CH_4 formation. Thus it is possible that CO chemisorption corresponds not to the real surface area of the Ni phase, but rather to the total CO uptake, which strongly depends on the catalytic properties of the surface, that is, its ability to adsorb strongly or weakly and dissociate CO or to be restructured when in contact with the chemisorbed gases [23]. As discussed later, Au has a detrimental effect on the catalytic properties of the low Au content Ni(Au 0.2 at%)/YSZ, and its behavior resembles that of Ni/YSZ.

Fig. 3 depicts the results of temperature-programmed reduction experiments carried out by TGA. The samples were heated linearly at a ramp rate of 20 K/min from 300 to 1123 K under 8% H_2/Ar flow (65 cc STP/min). As shown, the Au modified Ni/YSZ samples were reduced at temperatures even 150 K below the reduction temperature of Ni/YSZ itself [21]. In particular, Ni(Au 1 at%)/YSZ exhibited two overlapping peaks around the location of the peak maximum (∼630 K) which is 90 K below the H_2 reduction peak temperature (∼720 K) of the Ni(Au 0.2 at%)/YSZ. Thus, according to the aforementioned TGA experiments, it can be deduced that the lower reduction temperature of the Au-modified Ni/YSZ catalysts implies a weaker Ni–O bond.

Fig. 4 shows XPS measurements of Ni corresponding to the Ni2p photoelectrons of the two NiAu/YSZ samples. Before being transferred to the UHV system, the samples were prereduced at 1123 K for 1 h under H_2(5%)/He flow (100 cc STP/min). After prereduction, the samples were mounted on the atmospheric pressure prechamber/reactor, which was mounted onto the fast-entry system of the UHV system, where they were

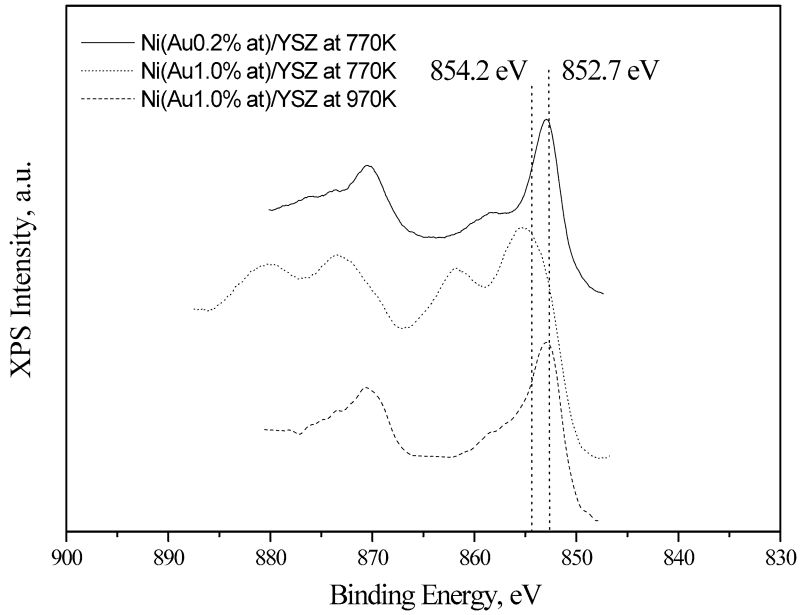

Fig. 4. XP spectra of Ni2p core level for the catalysts Ni(Au 0.2 at%)/YSZ at 770 K (—) and Ni(Au 1.0 at%)/YSZ at 770 K (···) and 970 K (- - -).

pretreated under pure H_2 flow (1 bar) at 1000 K for 10 min. Subsequently, the sample was evacuated and introduced directly into the analysis UHV chamber without being exposed to the atmosphere. The XP spectra were recorded while the samples were heated at 770 K. The spectrum recorded for Ni(Au 0.2 at%)/YSZ shows that Ni is in the metallic state, as expected because the samples were reduced under H_2 flow. Surprisingly, the spectrum of the Ni2p photoelectrons initially recorded at 770 K for the Ni(Au 1 at%)/YSZ sample shows that most of the Ni is in either the form of NiO (854.2 eV) or the form of $Ni(OH)_2$ (855.5 eV) [24]. Such behavior was reported by Zafeiratos and Kenou [25], who recorded the progressive oxidation of Ni or NiAu thin films deposited on YSZ when the samples were heated at 680 K under UHV conditions. This was attributed to the spillover of O species onto the Ni surface originating from the YSZ substrate. The evolution period of the aforementioned oxidation phenomenon was 3–4 h at 680 K for Ni thin (0.3–2 mm) films. The process became faster at higher temperatures. It is already well established that YSZ evolves oxygen and becomes a nonstoichiometric oxide at elevated temperatures [26–28]. Similarly, in the present case depicted in Fig. 4, the oxidation of Ni under UHV conditions at elevated temperature (770 K) can be attributed to the same process described earlier [25]. However, considering that the same procedure was followed for both samples, the different Ni oxidation states in the two catalysts can be attributed to the differences in oxygen mobility and evolution from the YSZ component. In this respect, it can be assumed that the higher Au content in the Ni(Au 1 at%)/YSZ sample induces more rapid kinetics for oxygen evolution from the YSZ particles. This strong interaction can be due to the nanostructure of the catalysts (see the particle sizes in Table 1), thus allowing for intimate contact and interference between the physicochemical properties of the NiAu and YSZ nanoparticles. As we discuss later, this property is beneficial for improving the carbon deposition resistance of the Ni(Au 1 at%)/YSZ. As shown in Fig. 4, on heating the sample at higher temperature (970 K), the oxide and hydroxide forms of Ni decompose into metallic Ni.

3.2. Equilibrium-dissociative adsorption of CH_4

The effect of Au content on the catalytic properties of Ni-based cermets was studied for the dissociative adsorption of CH_4. A typical equilibrium adsorption experiment is depicted in Fig. 5, which plots the amounts of deposited C, H_2 in the gas phase, and H species remaining on the surface, as well as the ratio of surface H/C deposited against temperature. The surface H/C ratio takes values between 3 and 0.5, depending on the temperature and the sample. In general, the sample with high Au content has a lower surface H/C ratio at elevated temperatures. As discussed later, the missing hydrogen is combined with C to form CH_x adsorbed species. Fig. 6 depicts the effect of P_{CH_4}/P_{H_2} and $P_{CH_4}/P_{H_2}^{3/2}$ on the amount of deposited C and the surface H/C ratios for Ni(Au 0.2 at%)/YSZ and Ni(Au 1 at%)/YSZ at various temperatures. The x-axis was chosen based on the average measured surface H/C ratio for the two samples. The lines passing through the experimental points depict two sets of equilibrium experiments where (a) the amount of CH_4 introduced into the reactor loop was varied isothermally and (b) a constant amount of CH_4 was introduced at various temperatures. It is clearly shown that the surface H/C ratios are around 2 and 1, respectively, indicating that CH_2 and CH species prevail on the Ni(Au 0.2 at%)/YSZ and Ni (Au 1 at%)/YSZ surfaces, respectively.

3.3. TPSR and TPO experiments

The nature of the carbon species created during the equilibrium adsorption of CH_4 was elucidated by carrying out TPSR and TPO experiments under H_2 flow and oxygen pulse, re-

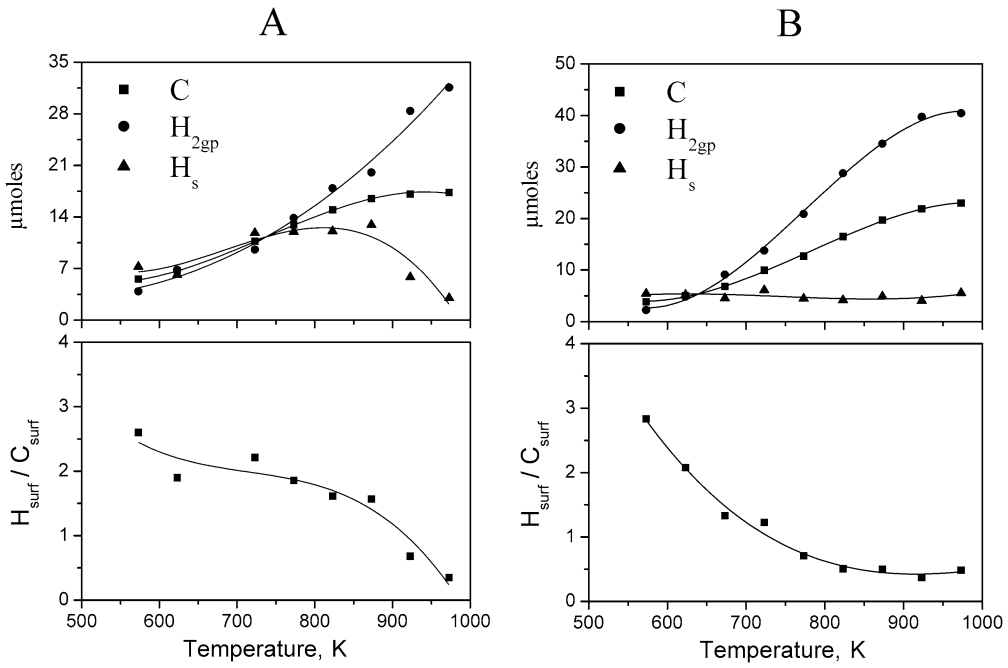

Fig. 5. Effect of temperature on the product distribution and surface H/C ratio during the equilibrium dissociative adsorption of CH_4 on Ni(Au 0.2 at%)/YSZ dosing $n_{CH_4} = 17.7$ μmol (A) and Ni(Au 1.0 at%)/YSZ dosing $n_{CH_4} = 24$ μmol (B). C: surface carbon, H_{2gp}: gas phase H_2, H_s: surface H species.

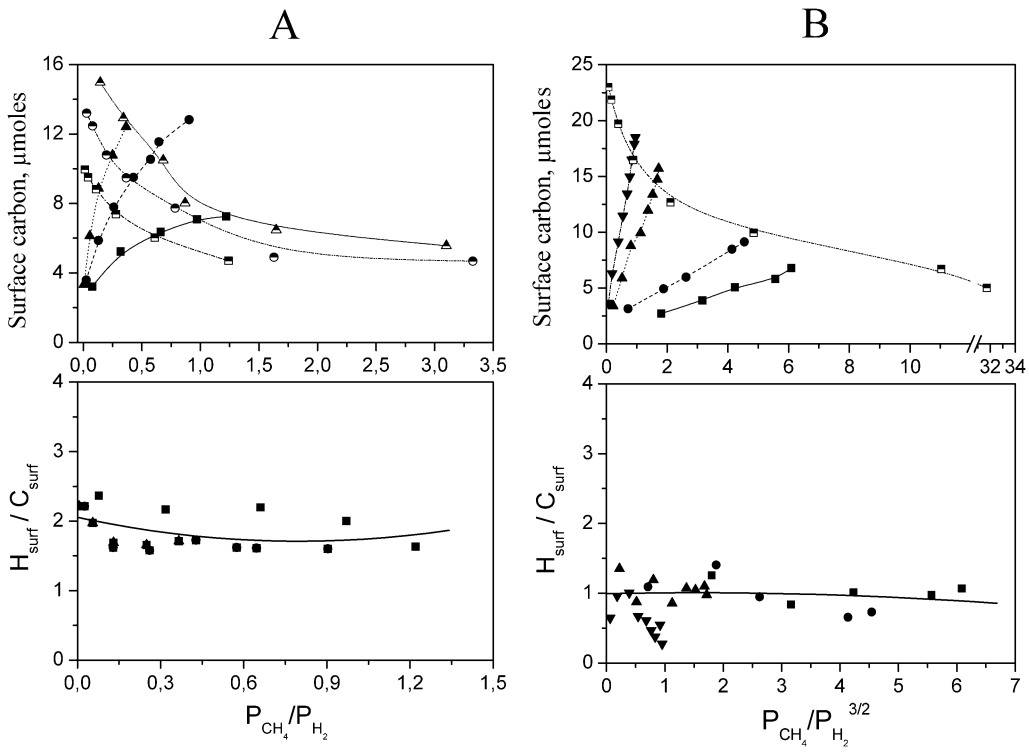

Fig. 6. Effect of equilibrium products of reaction 3 for Ni(Au 0.2 at%)/YSZ (A) and reaction 4 for Ni(Au 1 at%)/YSZ (B) on the amount of deposited C and the surface H/C ratio. Solid symbols correspond to isothermal experiments with various amounts of CH_4 at (■) 673, (●) 723, (▲) 773, and (▼) 823 K. Half-filled symbols correspond to experiments with constant amount of CH_4 at various temperatures: (⬒) 10, (◓) 14, and (◬) 17.7 μmol for Ni(Au 0.2 at%)/YSZ, (⬒) 24 μmol for Ni(Au 1 at%)/YSZ.

spectively (Figs. 7–9). Figs. 7 and 8 depict TPSR experiments under H_2 flow on Ni(Au 0.2 at%)/YSZ (Fig. 7) and Ni(Au 1.0 at%)/YSZ (Fig. 8). In both cases the carbon species formed during the dissociative equilibrium adsorption of CH_4 reacts with H_2 to produce CH_4 within broad temperature ranges, 300–650 K (Fig. 7) and 450–850 K (Fig. 8a), respectively. The spectra reveal the existence of four peaks (Fig. 7) and three peaks (Fig. 8) for the two samples, respectively, which can be easily

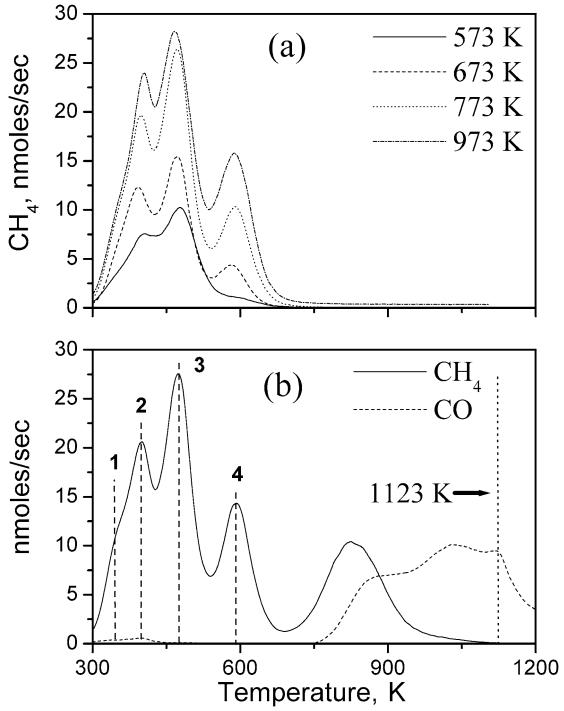

Fig. 7. TPSR spectra of surface carbon under 2.5% H_2/Ar flow, deposited during equilibrium dissociative adsorption of CH_4 (a) at different temperatures with initial amount of CH_4 17.7 μmol, and (b) at 773 K with initial amount of CH_4 59.6 μmol. Total flow rate 167 cc STP/min, ramp rate: 20 K/min. Catalyst Ni(Au 0.2 at%)/YSZ.

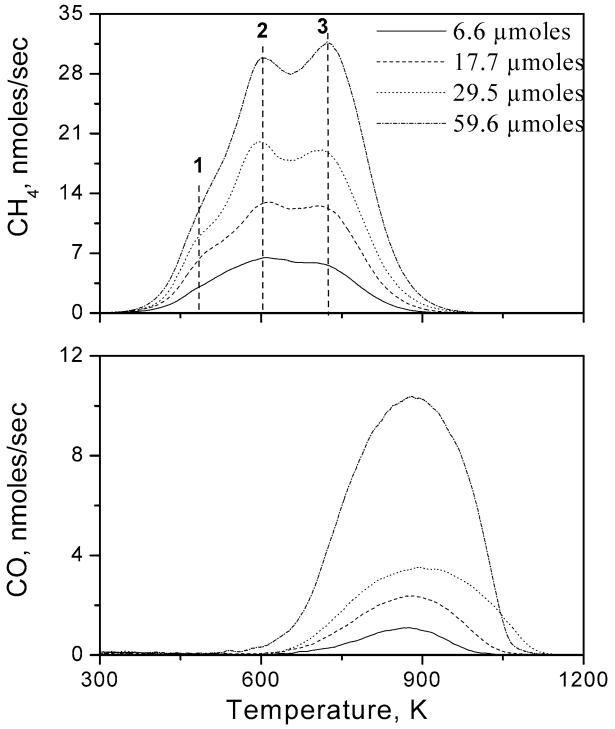

Fig. 8. TPSR spectra of surface carbon under 2.5% H_2/Ar flow, deposited during equilibrium dissociative adsorption of CH_4 at 823 K for different initial amounts of CH_4. Total flow rate 167 cc STP/min, ramp rate: 20 K/min. Catalyst Ni(Au 1.0 at%)/YSZ.

deconvoluted, corresponding to an equal number of adsorbed carbon species on the surface, most likely in the form of CH_x species. The arguments of this ascertainment are presented in Section 4. The main differences between the two samples are the different temperature ranges and the higher temperatures of CH_4 formation in the case of Ni(Au 1.0 at%)/YSZ. In a previous study of CH_4 dissociation on Ni/YSZ [21], these C species, the hydrogenation of which resulted in the formation of CH_4 within the temperature range of 300–650 K, were assigned to carbidic species on Ni surface, whereas the CO produced above 800 K was attributed to graphitic species oxidized by the oxidic species evolving from YSZ at high temperatures. CO has been also detected in the high-Au content sample (Fig. 8b), but as we discuss later, this should have originated from oxidation and decomposition of the hydrogenated carbon species.

Another significant difference in the behavior of the two samples is the appearance of the so-called "adsorbed carbon" species, which have been detected and characterized as such on Ni/YSZ [21] (Fig. 7b). These species appear when large amount of CH_4 is introduced in the reactor loop and are accompanied by the appearance of graphitic carbon at higher temperatures. In contrast, under the same conditions no such species were observed on the high-Au content sample, indicating the higher tolerance of Ni(Au 1 at%)/YSZ toward graphitic carbon deposition ($n_{CH_4} = 59.6$ μmol; Fig. 8).

The corresponding TPO experiments of the two samples are depicted in Fig. 9. The main products for both samples are CO_2, CO, and H_2. CO_2 desorbs above 500 K, with the peak maximum at 600 K for Ni(Au 0.2 at%)/YSZ and 680 K for

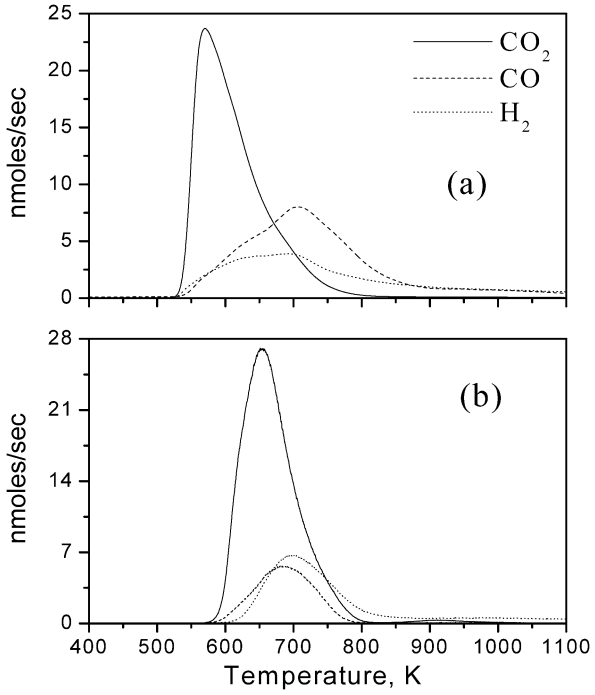

Fig. 9. Temperature-programmed oxidation (TPO) of surface carbon, deposited during equilibrium dissociative adsorption of CH_4 (a) on Ni(Au 0.2 at%)/YSZ at 773 K with initial amount of CH_4 17.7 μmol, and (b) on Ni(Au 1.0 at%)/YSZ at 723 K with initial amount of CH_4 24 μmol. Adsorbed O_2 quantity at room temperature is twice the amount of deposited surface carbon. Ramp rate: 20 K/min. Ar molar flow rate = 26 μmol/s.

Ni(Au 1.0 at%)/YSZ. The most interesting feature of the TPO experiments is the evolution of CO and H_2 within the same temperature range and at essentially the same peak temperature maximum (around 700 K). The simultaneous production of CO and H_2 shows that both gases originate from the dissociation of the same compound, such as oxyhydrogenated carbon species. As has already been concluded in a previous study on Ni/YSZ [21], CO_2 is formed via the oxidation of carbidic species. However, as we discuss in the next section, CO and H_2 production occurs through the surface oxidation of CH_x species to form oxyhydrogenated species and its subsequent dissociation at higher temperatures.

4. Discussion

In accordance with the conclusions of a previous study on the dissociative adsorption of CH_4 on Ni/YSZ [21], three types of carbon species have been detected that participate as either active reaction intermediates or catalyst deactivation agents:

- The carbidic species, which are highly reactive toward their hydrogenation to produce methane at 300–700 K.
- The adsorbed carbon species, which react with H_2 at temperatures as high as 800 K and can be considered the intermediate toward the formation of graphitic species.
- The graphitic species, which do not react with H_2 and are removed by oxygen at temperatures above 800 K. This species is well known in the literature as the main catalyst's deactivating agents.

Our experimental results show that the carbon/carbonaceous species on the NiAu/YSZ samples have similar features to those on Ni/YSZ. The main difference is localized on their reactivity with CH_4, CO, H_2, and O_2, which is attributed to the effect of Au on both the catalytic properties of Ni particles and their interaction with YSZ, the properties of which seem to be affected by the presence of gold, as shown in Figs. 3 and 4. In what follows, we explore the kinetic mechanisms that govern the partial and complete oxidation of CH_4 for synthesis gas and CO_2 production, respectively.

4.1. CH_x species

Based on the experimental evidence, we conclude that during the equilibrium dissociative adsorption of CH_4, CH_x species are formed and exist on the Ni surface. These can be considered in equilibrium with the formed carbidic species. The first evidence of the existence of CH_x species is the missing H_2 in the gas phase, which is not balanced to the equilibrium conversion of CH_4. As depicted in Fig. 5, especially at lower temperatures, the amount of H_2 remaining on the surface during the equilibrium adsorption of CH_4 corresponds to an H/C ratio starting at 3 and decreasing progressively with increasing adsorption temperature. This indicates that at higher temperatures, CH_x species with less H are mostly stable and in equilibrium with carbidic species. In addition, the TPSR experiments for both samples showed at least three distinct peaks located within a temperature window of 400 K (Figs. 7 and 8). The possibility that these peaks correspond to different carbidic species on the Ni surface is not in accordance with the TPO experiments (Fig. 9), which show only one CO_2 peak corresponding to its oxidation [21]. Thus it is plausible that during the exposure of the sample to H_2 flow at the beginning of the TPSR spectra, the various CH_x species are distributed on the Ni surface according to the established equilibrium between successive species. The position of the peak temperature is related to the chemical equilibrium between the CH_x species and their reactivity toward hydrogenation. In this respect, the deconvoluted peak areas can provide quantitative information on the distribution and qualitative information on the reactivity of the various CH_x species with H_2. Thus it is rational to assume that the low-temperature peak in Fig. 7 (peak 1) corresponds to adsorbed CH_4, whereas CH corresponds to the CH_4 peak evolving at 585 K. However, in Ni(Au 1 at%)/YSZ, adsorbed CH_4 species are not likely to survive and desorb at higher temperatures, and thus the three deconvoluted peaks may correspond to CH_3, CH_2, and CH species. Table 3 gives the correspondence of the various peak maximum temperatures to the respective CH_x species for the two samples under study.

Table 3
Peak maximum temperatures of the respective CH_x species for the two catalysts, determined by the deconvolution of the TPSR experiments of Figs. 7 and 8

Ni/Au-YSZ	Peak maximum temperature (K)			
	CH_4	CH_3	CH_2	CH
0.2 at% Au	345 (1)[a]	400 (2)	475 (3)	585 (4)
1.0 at% Au	–	500 (1)	595 (2)	710 (3)

[a] Numbers in parentheses correspond to the labeled peaks of Figs. 7 and 8.

The fact that in all cases the corresponding CH_4 desorbing temperatures of the Ni(Au 1 at%)/YSZ are at least 100 K above those of Ni(Au 0.2 at%)/YSZ indicates that a higher Au quantity lowers the reactivity of the Ni surface to hydrogenate carbidic and CH_x species toward CH_4 formation. Lower reactivity of the surface denotes higher stability of the reacting adsorbed species. The stability of the reacting species on the surface can be realized due to a higher activation barrier (kinetic considerations) or stronger bonding/interaction of the species with catalytic surface (thermodynamic considerations). To clarify the contribution of these two factors on the C-tolerant properties of the Ni(Au 1 at%)/YSZ, the isosteres for the two catalysts are plotted for various coverages of the adsorbed carbonaceous species (Fig. 10). The isosteres were derived on the basis of the equilibrium experiments depicted in Fig. 6 and on the assumption that during the equilibrium dissociative adsorption of CH_4, CH_x species is adsorbed mainly on the catalytic surface, whereas x is generally determined by estimating the ratio of surface H to surface C as is experimentally derived from the mass balances during the equilibrium experiments (Figs. 5 and 6). Thus, the following overall reactions on the Ni(Au 0.2 at%)/YSZ and Ni(Au 1 at%)/YSZ catalysts can be considered:

$$CH_4 \Leftrightarrow (CH_2)_{ad} + H_2 \quad (3)$$

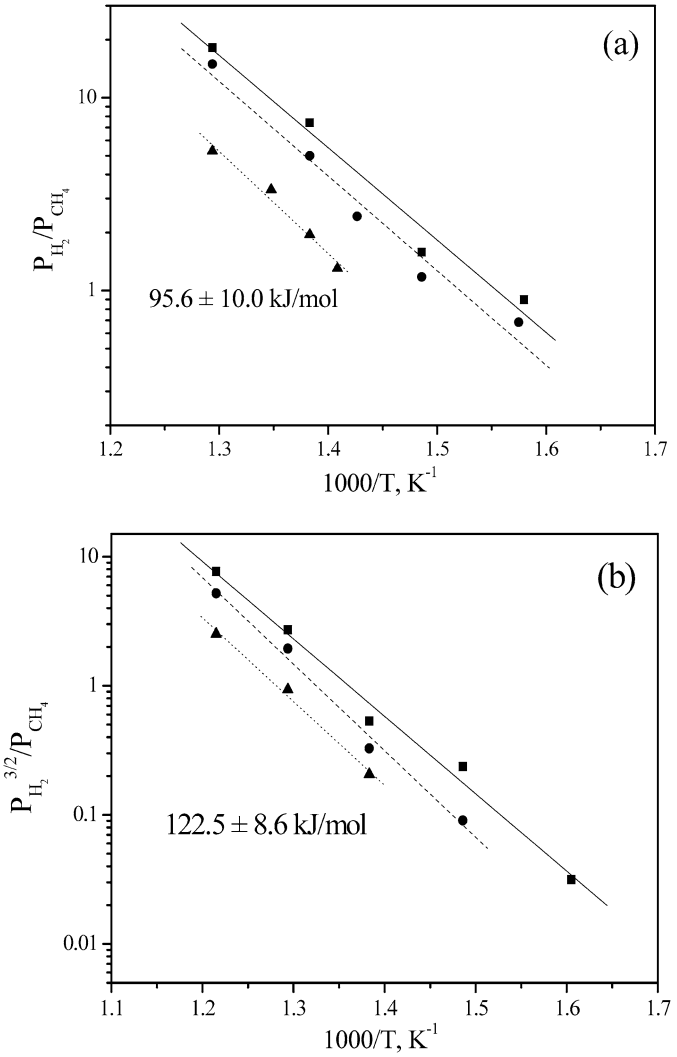

Fig. 10. Isosteres for CH_4 equilibrium dissociative adsorption corresponding to 5 (■), 6.8 (●) and 10 (▲) μmol of surface carbon on (a) Ni(Au 0.2 at%)/YSZ and (b) Ni(Au 1.0 at%)/YSZ, based on the experimental data of Fig. 5.

and

$$CH_4 \Leftrightarrow (CH)_{ad} + \frac{3}{2}H_2. \quad (4)$$

The slopes of the isosteres in Fig. 10 correspond to the enthalpy change of reactions (3) (95.6 kJ/mol) and (4) (122.5 kJ/mol) and qualitatively express the binding strength of the adsorbed CH_x species on the catalytic surface. In this respect, the adsorbed CH species on Ni(Au 1 at%)/YSZ resulting from reaction (4) are less strongly bonded onto the catalytic surface than the corresponding CH_2 species on Ni(Au 0.2 at%)/YSZ. Taking into account these considerations, we come to the conclusion that the higher hydrogenation temperature of CH_x species on the Ni(Au 1 at%)/YSZ surface, as shown in the TPSR experiments of Fig. 8, can be attributed to the increased activation barriers of the hydrogenation reactions. This also implies lower binding energy of the intermediate activated complexes. CH_4 dissociation accompanied by the successive dehydrogenation steps in the formation of CH_x species on the surface should experience similar increases in activation barriers, resulting in a decreased rate of CH_4 dehydrogenation on the Ni(Au 1 at%)/YSZ surface and subsequently a lifetime elongation of the CH_x species on the catalytic surface.

In accordance with the present observations, Besenbacher et al. [22] were the first to show by theoretical DFT calculations and experimental measurements that small amounts of Au on the Ni surface increase the resistance toward graphite formation either by increasing the activation barrier of CH_4 dehydrogenation reaction or by decreasing the binding energy of the resulting CH_x and C species on the Ni surface. The foregoing considerations are also corroborated by both the temperature-programmed reduction experiments (Fig. 3) and the surface titration experiments (Fig. 2). In the first case, it was shown that NiO was reduced at lower temperature on Ni(Au 1 at%)/YSZ than on Ni(Au 0.2 at%)/YSZ, indicating weaker bonding of Ni with O. In addition, the chemisorption of CO on the high-Au content sample did not result in its dissociative adsorption toward the formation of carbidic carbon and adsorbed O_{ad}. This is demonstrated by the fact that little CH_4 was produced during the TPSR experiment depicted in Fig. 2 in the case of Ni(Au 1 at%)/YSZ. This can be attributed to the weaker bonding of CO with the Ni surface and, consequently, the lower degree of electron back-donation at the C=O $2\pi^*$ antibonding orbital. The strong interaction of $2\pi^*$ antibonding orbital with the surface metallic d-band may cause destabilization of the C=O bond, possibly resulting in disruption of the bond and formation of carbidic and oxidic species on the Ni surface [29].

Fig. 11 depicts the distribution of the CH_x species on the surface of the two samples as derived by deconvolution of the TPSR experiments depicted in Figs. 7 and 8. On both samples, the most abundant species is CH_2; on Ni(Au 1 at%)/YSZ, CH species is almost as abundant as CH_2. The distribution of the various CH_x species depends only on the amount/coverage of the carbidic species formed on the surface regardless of the temperature at which the dissociative equilibrium adsorption of methane occurred. In this respect, the distribution of the various CH_x species does not necessarily reflect the distribution of the species during the equilibrium adsorption of CH_4; however, their distribution does indicate qualitatively the prevailing species on the surface of the two samples.

The sequential dehydrogenation of CH_4 has been studied extensively both theoretically [30–36] and experimentally [37–41]. In general, it is well established that the dissociative adsorption of CH_4 is an activated process whereby H_2 is progressively abstracted with varying activation energy at each H removal. The calculated [30–32,34,36] and experimentally measured [37,40,41] activation energy for CH_3 formation lies between 70 and 100 kJ/mol, whereas activation energies for the formation of the rest of CH_x species vary between 30 and 100 kJ/mol [34,36]. Bengaard et al. [42] reported that CH_4 activation occurs on stepped surfaces and that the most stable species was calculated to be ($CH^* + 3H^*$), which exhibits the lowest energy of all CH_x species, as well as the highest activation barrier toward the formation of adsorbed ($C^* + 4H^*$).

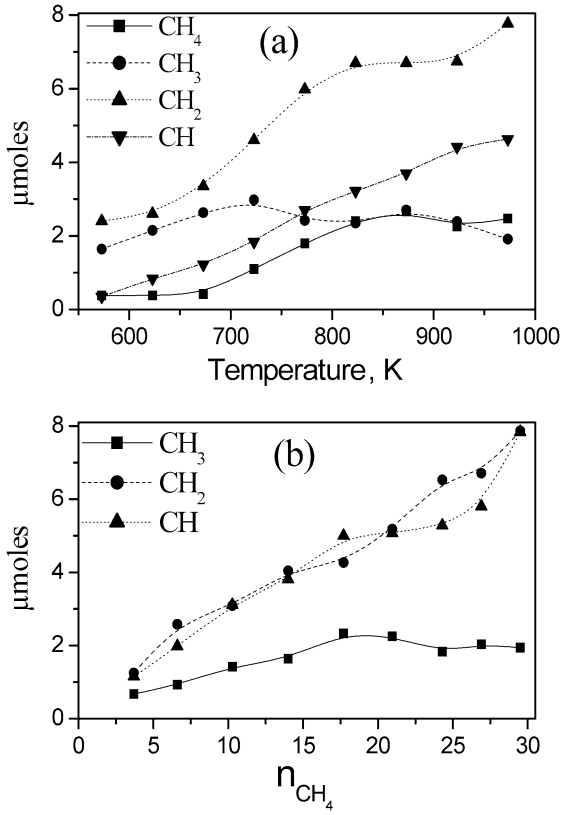

Fig. 11. Distribution of CH_x species on the surface of (a) Ni(Au 0.2 at%)/YSZ with increasing temperature and (b) Ni(Au 1.0 at%)/YSZ with increasing methane dose in the reactor loop, based on the deconvolution of the TPSR experiments depicted in Figs. 7 and 8, respectively. The correspondence of the peak maxima of the deconvoluted peaks to the adsorbed CH_x species is shown in Table 3.

4.2. Oxidation of the CH_x species

In contrast to the multiple CH_4 TPSR peaks, the TPO experiments (Fig. 9) detected one CO_2 peak. The most interesting feature is the simultaneous production of CO and H_2, demonstrating that both gases originate from the dissociation of one species adsorbed on the Ni surface. This observation can be interpreted by considering that the species left on the surface after purging the catalytic bed with Ar flow are carbidic species in equilibrium with the most stable CH_x species. Their interaction with adsorbed O_{ad} species results in the preferential production of CO_2 and the formation of adsorbed oxyhydrogenated species, the latter of which are decomposed at higher temperatures into CO and H_2. It is noteworthy that no water production occurs, demonstrating the lack of adsorbed H_{ad}, which would react with O_{ad} toward H_2O formation. Thus, according to the above considerations, the following reactions occur:

$$C_c + 2O_{ad} \rightarrow CO_2, \tag{5a}$$

$$CH_x + O_{ad} \rightarrow CH_xO_{ad}, \tag{5b}$$

and

$$CH_xO_{ad} \rightarrow CO + \frac{x}{2}H_2. \tag{5c}$$

The calculated H_2/CO ratio corresponding to the amounts of H_2 and CO evolved during the TPO experiments can be considered a stability indicator of the CH_x species on the surface. Thus, the Ni(Au 0.2 at%)/YSZ and Ni(Au 1 at%)/YSZ H_2/CO ratios have average values of 0.58 and 1.25, respectively. This strongly indicates that the stable CH_x species contain larger numbers of H atoms on Ni(Au 1 at%)/YSZ than on Ni(Au 0.2 at%)/YSZ, implying that the former sample is less reactive toward the dehydrogenation of CH_4 and CH_x species, in accordance to the same conclusion reached earlier based on the TPSR experiments (Figs. 7 and 8).

Based on the foregoing discussion and on the fact that YSZ evolves oxygen at temperatures over 600 K, which can oxidize adsorbed carbonaceous species, the CO evolved during the TPSR experiments of Fig. 8 on Ni(Au 1 at%)/YSZ at temperatures of 600–1000 K with a peak maximum at 900 K can be attributed to the thermal decomposition of CH_xO_{ad}. These species can be formed on the Ni(Au 1 at%)/YSZ due to the higher stability of CH_x species at higher temperatures and their oxidation by the evolved O_2 from YSZ. It is noteworthy that CO production is detected at temperatures as low as 600 K only on the high-Au content catalyst, whereas on Ni(Au 0.2 at%)/YSZ, CO is detected at temperatures above 800 K and is related to oxidation of the graphitic species formed on the catalysts when a large amount of CH_4 is introduced in the reactor loop (Fig. 7b). Beyond the fact that CH_x species can survive at higher temperatures on Ni(Au 1 at%)/YSZ, their oxidation into CH_xO_{ad} species at lower temperatures and subsequent decomposition accompanied by CO evolution must be related to the effect of Au addition on enhancing oxygen evolution from the YSZ particles at lower temperatures. In this respect, it can be concluded that the addition of Au promotes the role of YSZ as an oxidizing supporting material even at temperatures as low as 600 K, in accordance with earlier conclusions based on the XPS measurements of Fig. 4.

4.3. Kinetics of CH_4 partial oxidation and steam-reforming reactions

The kinetics of the partial oxidation of methane toward the production of synthesis gas on Ni and several other metal-supported catalysts has been the subject of numerous studies [43–51]. The main kinetic characteristic of the process is the low selectivity toward CO and H_2 at low temperatures (<873 K), where the process selectively produces CO_2 and H_2O [51]. It is well established that CH_4 activation/dehydrogenation is the rate-determining step for the reaction of CH_4 consumption in partial oxidation and reforming reactions of CH_4 [52]; however, the selectivity toward CO, CO_2, H_2, and H_2O formation must depend on the relative reactivity of intermediate steps at the various temperatures, which may result in either complete or partial oxidation products. According to the preceding discussion, we reach the conclusion that the selectivity toward CO oxidation depends on two factors: (1) the lifetime and surface concentration of CH_x species and (2) the decomposition temperature of the CH_xO species.

Although the surface concentration of CH_x species is higher at low temperatures, the low decomposition rate of the CH_xO species formed at these low temperatures can be considered the

main reason (i.e., limiting step) for the low CO selectivity at low temperatures. Thus the complete oxidation of carbidic species, which is very reactive at low temperatures, leads to the formation of CO_2 rather than CO. With increasing temperature and especially at temperatures as high as 973 K, the decomposition rate of CH_xO species is sufficiently high, and the selectivity now depends on the stability of the CH_x species; thus, their high surface concentration will result in the formation of CH_xO species with higher reaction rate than the formation of carbidic and sequentially adsorbed C, which will lead to either CO_2 production or graphite deposition on the catalyst. Similar kinetic considerations can be proposed for the steam-reforming reaction of CH_4. In a kinetic investigation of the CH_4 steam-reforming reaction, Xu and Froment [53] proposed that the oxidation of CH_2 species to form adsorbed CH_2O_{ad} is the limiting step of the reaction.

Several researchers have proposed the oxidation of CH_x toward the production of CO and H_2 as a possible pathway for synthesis gas production [47–49,54–56]. Osaki et al. [54] and, more recently, Wu et al. [56] used pulse surface reaction rate analysis in studies of CH_4–CO_2 reforming and CH_4 partial oxidation and concluded that various CH_x intermediates present on Ni-supported catalysts react with adsorbed O_{ad} species in the production of CO. During pulsing of CH_4/Ar over the catalyst, CO and H_2 exhibit longer tailing responses, indicating that CH_x species are present on the catalytic surface. These authors concluded that the reaction over the reduced catalyst occurs via the direct surface oxidation mechanism, which involves adsorbed CH_x and oxygen species.

In accordance with the foregoing discussion, we propose the following kinetic model to describe the partial oxidation of methane toward the production of synthesis gas:

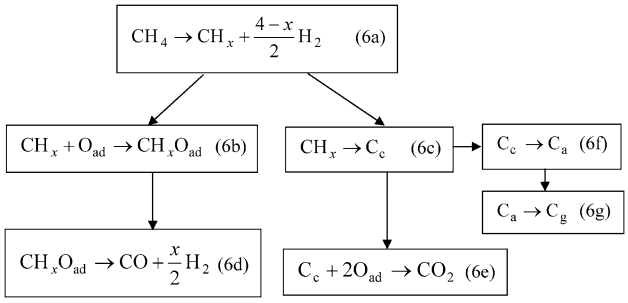

(6)

This model can also be valid for the steam-reforming reaction. In this mechanism, O_{ad} can be supplied by O_2 adsorption (partial oxidation), H_2O dissociative adsorption (steam reforming), or electrochemically through an O^{2-} conductor like YSZ (electrochemical oxidation in SOFC).

Reaction steps (6f) and (6g) show the sequences toward the formation of adsorbed carbon species (C_a) and graphite (C_g) [21]. C_a is a reactive C species with both H_2 and O_2 but at higher temperatures (>800 K) than carbidic C_c [21]. The formation of C_a gives rise to the formation of the graphitic layer as well. The rates of C_a and C_g formation depend on the dissociation rate of the CH_x species and the nucleation rate of the C_a species, respectively.

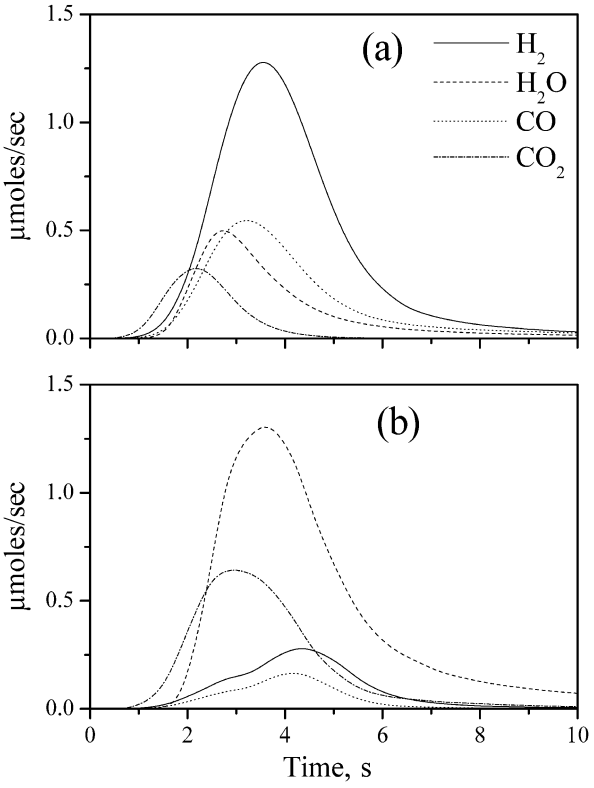

Fig. 12. Products distribution during a pulse of 2.2 μmol CH_4 at 973 K over preoxidised Ni-YSZ with (a) 2.1 and (b) 4.4 μmol O_2.

The foregoing kinetic considerations are corroborated by the pulse experiment depicted in Fig. 12. A 2.2-μmol CH_4 pulse was introduced into a catalytic bed of 50 mg Ni/YSZ onto which O_2 was preadsorbed by pulsing 2.1 μmol O_2 (Fig. 12a). As shown, first CO_2 is produced, followed by H_2O formation. The peaks of CO and H_2 appear to be wider and to have longer tails just after the water peak, whereas the fact that they appear simultaneously indicates (as concluded above) that they originate from the decomposition of the same surface species (CH_xO_{ad}). The delayed appearance compared with the earlier appearance of CO_2 demonstrates that the decomposition of the CH_xO species into CO and H_2 proceeds with lower reaction rates compared with the faster oxidation of the carbidic C_C species into CO_2 [21]. It is noteworthy that the evolution of water is not related to the evolution of the CO_2 peak, demonstrating that water is formed independently by the oxidation of H species originating from the dehydrogenation of CH_4. It is also interesting that the pulse of the same quantity of CH_4 over Ni/YSZ, on which a larger amount of O_2 (4.4 μmol) was preadsorbed, shows the formation of broadened CO_2 and H_2O peaks (Fig. 12b). The broadening of the peaks in contrast to CO_2 and H_2O peaks in Fig. 12a can be attributed to the oxidation by the excess O_{ad} of the CO and H_2 produced by the delayed decomposition of CH_xO species. Thus in the case of excess O_2, the complete oxidation of CH_xO species into CO_2 and H_2O proceeds through the decomposition/oxidation processes according to the following reaction scheme:

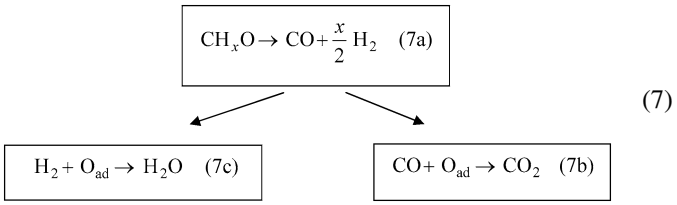

(7)

4.4. The effect of Au

Based on our experimental results and their interpretation, we conclude that adding a critical amount of Au onto the Ni catalyst affects the reactivity of the Ni surface toward CH_4 activation by impeding the dehydrogenation and hydrogenation reactions, as well as the oxidation of the carbonaceous species formed on the catalytic surface. Using DFT calculations, Besenbacher et al. [22] showed that adding a small amount of Au increases the resistance toward graphite formation. Based on their calculations, they concluded that Au induces such changes on the catalytic/electronic properties of the Ni surface so that both the activation barrier of CH_4 dehydrogenation and the energy of the resulting carbon/carbonaceous species increase, thus inhibiting graphite formation. More recently, Bengaard et al. [42] carried out more detailed DFT calculations in combination with kinetic measurements and microkinetic simulations on the activation of CH_4 and the effect of catalysts promoters of the Ni surface (e.g., S, K, and Au) on the catalytic rate. They concluded that the highly reactive sites for both CH_4 activation and graphite nucleation are located on the step edges of Ni on which the aforementioned promoters preferentially bind. Thus the optimized catalyst should accommodate just enough promoter so that graphite formation is effectively blocked while methane activation and its reforming by steam occurs at an appreciable rate.

5. Conclusions

The main conclusions derived from the present study can be summarized as follows:

- The addition/decoration of the Ni surface with a very small quantity of Au ($\leqslant 1$ at% with respect to Ni) inhibits the formation of graphitic carbon.
- The presence of Au results in a decreased rate of CH_4 dehydrogenation and an increase in the lifetime, stability, and surface concentration of CH_x species.
- The partial oxidation of CH_4 into synthesis gas can be attributed to the oxidation of adsorbed CH_x species into CH_xO_{ad} and its subsequent dissociation into H_2 and CO at higher temperatures (700 K).
- The complete oxidation toward CO_2 formation proceeds selectively through the reaction of carbidic carbon, which is a rather fast process even at temperatures as low as 500 K.

Based on the foregoing considerations, the NiAu/YSZ catalyst is expected to be a highly carbon tolerant and selective catalyst/electrode in the CH_4 partial oxidation reaction for the production of synthesis gas. In addition, its carbon tolerant properties can be beneficial for water lean steam-reforming conditions, a particularly desirable property for the internal steam reforming of CH_4 in solid oxide fuel cells.

Acknowledgment

This work was supported by the INCO2-COPERNICUS2 programme of the European Commission under contract ICA2-CT-2000-10003.

References

[1] E.P. Murray, T. Tsai, S.A. Barnett, Nature 400 (1999) 649.
[2] A. Atkinson, S. Barnett, R.J. Gorte, J.T.S. Irvine, A.J. McEvoy, M. Mogensen, S.C. Singhal, J. Vohs, Nature Mater. 3 (2004) 17.
[3] V. Antonucci, P.L. Antonucci, A.S. Aricò, N. Giordano, J. Power Sources 62 (1996) 95.
[4] T. Ishihara, T. Yamada, T. Akbay, Y. Takita, Chem. Eng. Sci. 54 (1999) 1535.
[5] V.V. Galvita, V.D. Belyaev, A.K. Demin, V.A. Sobyanin, Appl. Catal. A: Gen. 165 (1997) 301.
[6] C. Lu, W.L. Worrell, C. Wang, S. Park, H. Kim, J.M. Vohs, R.J. Gorte, Solid State Ionics 152–153 (2002) 393.
[7] J. Liu, S.A. Barnett, Solid State Ionics 158 (2003) 11.
[8] A. Weber, B. Sauer, A.C. Müller, D. Herbstritt, E. Ivers-Tiffée, Solid State Ionics 152–153 (2002) 543.
[9] J.B. Wang, J.-C. Jang, T.-J. Huang, J. Power Sources 122 (2003) 122.
[10] A. Abudula, M. Ihara, H. Komiyama, K. Yamada, Solid State Ionics 86–88 (1996) 1203.
[11] T. Horita, N. Sakai, T. Kawada, H. Yokokawa, M. Dokiya, J. Electrochem. Soc. 143 (1996) 1161.
[12] I. Alstrup, T. Tavares, J. Catal. 139 (1993) 513.
[13] R.T. Baker, I.S. Metcalfe, Ind. Eng. Chem. Res. 34 (1995) 1558.
[14] T.V. Choudhary, C. Sivadinarayana, C.C. Chusuei, A. Klinghoffer, D.W. Goodman, J. Catal. 199 (2001) 9.
[15] Z.L. Zhang, X.E. Verykios, Catal. Today 21 (1994) 589.
[16] M.L. Goula, A.A. Lemonidou, A.M. Efstathiou, J. Catal. 161 (1996) 626.
[17] J.S. Tsang, S.E. Park, H. Chon, Appl. Catal. A 145 (1996) 111.
[18] T. Borowiecki, A. Golebiowski, Catal. Lett. 25 (1994) 309.
[19] T. Borowiecki, G. Giecko, M. Panczyk, Appl. Catal. A: Gen. 230 (2002) 85.
[20] J.R. Rostrup-Nielsen, L. Alstrup, Catal. Today 53 (1999) 311.
[21] N.C. Triantafyllopoulos, S.G. Neophytides, J. Catal. 217 (2003) 324.
[22] F. Besenbacher, I. Chorkendorff, B.S. Clausen, B. Hammer, A.M. Molenbroek, J.K. Nørskov, I. Stensgaard, Science 279 (1998) 1913.
[23] M. Agnelli, M. Kolb, C. Mirodatos, J. Catal. 148 (1994) 9.
[24] D. Briggs, M.P. Seah (Eds.), Practical Surface Analysis, vol. 1, second ed., Wiley, New York, 1990, p. 201.
[25] S. Zafeiratos, S. Kenou, Surf. Sci. 532 (2003) 402–408.
[26] J. Xue, R. Dieckmann, in: T.A. Ramanarayanan, W.L. Worrel, H.L. Tuller (Eds.), Proc. of the 2nd Int. Symp. on Ionic and Mixed Ceramics, vol. 94-12, The Electrochemical Society, Pennington, NJ, 1994, p. 191.
[27] R. Dieckmann, J. Phys. Chem. Solids 59 (4) (1998) 507.
[28] S.G. Neophytides, D. Tsiplakides, C.G. Vayenas, J. Catal. 178 (1998) 414–428.
[29] B. Hammer, J.K. Nørskov, Adv. Catal. 45 (2000) 71.
[30] H. Yang, J.L. Whitten, Surf. Sci. 255 (1991) 193.
[31] H. Yang, J.L. Whitten, J. Chem. Phys. 96 (1992) 5529.
[32] H. Burghgraef, A.P.J. Jansen, R.A. van Santen, J. Chem. Phys. 101 (1994) 11012.
[33] P. Kratzer, B. Hammer, J.K. Nørskov, J. Chem. Phys. 105 (1996) 5595.
[34] H. Burghgraef, A.P.J. Jansen, R.A. van Santen, Surf. Sci. 324 (1995) 345.
[35] R.M. Watwe, H.S. Bengaard, J.R. Rostrup-Nielsen, J.A. Dumesic, J.K. Nørskov, J. Catal. 189 (2000) 16.
[36] C.T. Au, M.S. Liao, C.F. Ng, J. Phys. Chem. 102 (1998) 3959.

[37] M.B. Lee, Q.Y. Yang, S.L. Tang, S.T. Ceyer, J. Chem. Phys. 85 (1986) 1693.
[38] Q.Y. Yang, A.D. Johnson, K.L. Maynard, S.T. Ceyer, J. Am. Chem. Soc. 111 (1989) 8748.
[39] S.T. Ceyer, Langmuir 6 (1990) 82.
[40] T.P. Beebe, D.W. Goodman, B.D. Kay, J.T. Yates, J. Chem. Phys. 87 (1987) 2305.
[41] R.A. Campbell, J. Szanyi, P. Lenz, D.W. Goodman, Catal. Lett. 17 (1993) 39.
[42] H.S. Bengaard, J.K. Nørskov, J. Sehested, B.S. Clausen, L.P. Nielsen, A.M. Molenbroek, J.R. Rostrup-Nielsen, J. Catal. 209 (2002) 365.
[43] S.C. Tsang, J.B. Claridge, M.L.H. Green, Catal. Today 23 (1995) 3.
[44] Y. Lu, J. Xue, C. Yu, Y. Liu, S. Shen, Appl. Catal. A: Gen. 174 (1998) 121.
[45] R. Jin, Y. Chen, W. Li, W. Cui, Y. Ji, C. Yu, Y. Jiang, Appl. Catal. A: Gen. 201 (2000) 71.
[46] E. Ruckenstein, Y.H. Hu, Appl. Catal. A: Gen. 183 (1999) 85.
[47] A. Shamsi, Appl. Catal. A: Gen. 277 (2004) 23.
[48] W.-S. Dong, H.-S. Roha, K.-W. Jun, S.-E. Park, Y.-S. Ohb, Appl. Catal. A: Gen. 226 (2002) 63.
[49] K. Nakagawa, N. Ikenaga, T. Kobayashi, T. Suzuki, Catal. Today 64 (2001) 31.
[50] J.B. Claridge, A.P.E. York, A.J. Brungs, C. Marquez-Alvarez, J. Sloan, S.C. Tsang, M.L.H. Green, J. Catal. 180 (1998) 85.
[51] C. Elmasides, D.I. Kondarides, S.G. Neophytides, X.E. Verykios, J. Catal. 198 (1) (2001) 195.
[52] J. Wei, E. Iglesia, J. Catal. 224 (2004) 370–383.
[53] J. Xu, G.F. Froment, AIChE J. 35 (1989) 88.
[54] T. Osaki, H. Masuda, T. Mori, Catal. Lett. 29 (1994) 33.
[55] M.C.J. Bradford, M.A. Vannice, Appl. Catal. A: Gen. 142 (1996) 73.
[56] T. Wu, Q. Yan, H. Wan, J. Mol. Catal. A: Chem. 226 (2004) 41.